Dual-Layer Hollow Fibers with Enhanced Flux As Novel Forward Osmosis Membranes for Water Production

ARTICLE *in* ENVIRONMENTAL SCIENCE AND TECHNOLOGY · MAY 2009

Impact Factor: 5.33 · DOI: 10.1021/es803360t · Source: PubMed

3 AUTHORS, INCLUDING:

Tai-Shung Chung
National University of Singapore
727 PUBLICATIONS **19,578** CITATIONS

SEE PROFILE

Environ. Sci. Technol. **2009,** *43,* 2800–2805

Dual-Layer Hollow Fibers with Enhanced Flux As Novel Forward Osmosis Membranes for Water Production

QIAN YANG,[†] KAI YU WANG,[†] AND TAI-SHUNG CHUNG*[,†,‡]

Department of Chemical and Biomolecular Engineering, National University of Singapore, Singapore 119260, and Singapore-MIT Alliance, National University of Singapore, Singapore 119260

Received November 26, 2008. Revised manuscript received February 12, 2009. Accepted February 13, 2009.

We have demonstrated in this work the prospect of dual-layer polybenzimidazole-polyethersulfone (PBI-PES) nanofiltration (NF) hollow fiber membranes in the forward osmosis (FO) process for water production: The state-of-the-art for dual-layer membrane fabrication via coextrusion technology could produce the resultant membrane consisting of an ultrathin selective skin, fully porous water channels underneath, and a microporous sponge-like support structure. Together with its sharp pore size distribution and self-charged PBI selective membrane surface, the dual-layer hollow fiber forward osmosis membrane can achieve a water flux as high as 33.8 $L \cdot m^{-2} \cdot hr^{-1}$ and a salt flux less than 1.0 $g \cdot m^{-2} \cdot hr^{-1}$ at room temperature of 23 °C using 5 M $MgCl_2$ as the draw solution. A comprehensive literature review of previous efforts on identifying suitable membranes and appropriate draw solutions in the FO process for water production and seawater desalination have also been conducted. It shows that the water fluxes of the dual-layer hollow fiber FO membrane developed in this work utilizing $MgCl_2$ as the draw solutions generally surpasses those FO processes utilizing RO membranes and is comparable to most FO processes using commercial FO membrane and employing other salts or sugar instead of $MgCl_2$ as the draw solutions.

Introduction

To solve or alleviate the global water scarcity problem, tremendous effort has been put forth to identify novel methods of purifying wastewater or seawater at lower expenditure with less energy consumption. Forward (or direct) osmosis (FO), an emerging process for water reuses, seawater desalination as well as for dewatering aqueous streams with very little energy consumption, has recently received growing attention from numerous disciplines, such as water reclamation, wastewater treatment, seawater desalination, concentration of liquid foods, the controlled release of drugs via osmotic pumps, power generation, water purification, and reuse in space (*1*). Similar to reverse osmosis (RO), FO utilizes a selectively permeable membrane to separate water from dissolved solute molecules or ions. Nevertheless, instead of employing a hydraulic pressure as the driving force for the separation in the RO process, FO uses the chemical potential across the membrane, that is the osmotic pressure gradient, to induce a net flow of water through the membrane into the draw solution. Thus, FO may offer the advantages of the same high rejection of a wide range of contaminants and lower membrane-fouling propensities than traditional pressure-driven membrane processes. However, the major hurdles to fully explore FO potential as a new generation water production technology are (1) the limited number of commercially available FO membranes with high water permeation and superior salt separation performance; (2) the lack of desirable draw solutions which can be easily and directly separated from the extracted water with low energy expenditure; and (3) the optimization of the FO process to its maximum theoretical efficiency.

To overcome these hurdles, we aim to develop superior FO membranes capable of high water flux and high salt rejection. Without development of an appropriate membrane, FO is unlikely to materialize as a viable alternative water production technology. In our previous work, we have demonstrated for the first time polybenzimidazole (PBI) nanofiltration (NF) hollow fiber membranes with a small pore size and a narrow pore size distribution can be used in the FO process for water reclamation (*2*). The self-charged characteristics of PBI and its superior hydrophilicity make it less susceptible for membrane fouling and provide great potential for water reuses. However, the water permeation flux of the aforementioned PBI NF hollow fiber membrane was not satisfactorily high. This was due to the resultant single-layer membrane possessing a thick dense PBI selective layer and a tight substructure. The latter was probably resulted from the high viscosity nature of PBI dopes.

To substantially lower the substructure resistance of the resultant membranes, a new strategy is proposed and demonstrated in this work via a synergetic combination of dual-layer membrane fabrication and molecular engineering of polyethersulfone-polyvinylpyrrolidone (PES-PVP) blends as the supportive inner-layer. Dual-layer hollow fiber membranes have the advantage of maximizing membrane performance by using an extremely high-performance or functional membrane material as the selective layer, like PBI in our studies, and employing a low-cost material as the supporting layer, thus significantly reducing the overall production costs (*3*−*6*). To be applicable in FO processes for water production, molecular engineering design of the inner-layer is essential to achieve a fully porous open-cell structure with substantial hydrophilicity. Polyethersulfone (PES) is selected because of its tendency to form porous and open-cell structure with good mechanical properties, whereas the incorporation of polyvinylpyrrolidone (PVP) is needed to modify the hydrophobic nature of PES (*7*).

In this work we aim to achieve the dual-layer hollow fiber membrane with a narrow nanopore size distribution and an ultrathin selective outermost skin for water production with high throughput and purity in the forward osmosis process. For this proof-of-concept demonstration in which the dual-layer hollow fiber NF membrane could provide another platform for FO membrane development, the chosen feed and draw solutions were limited to deionized water and $MgCl_2$ solution, respectively. Overall FO process viability hinges on the successful integration of the osmotic step with a draw solute recovery process which may involve membrane distillation (MD) or reverse osmosis (RO). These processes

* Corresponding author phone: +65-65166645; fax: +65-67791936; e-mail: chencts@nus.edu.sg.
[†] Department of Chemical and Biomolecular Engineering.
[‡] Singapore-MIT Alliance.

10.1021/es803360t CCC: $40.75
Published on Web 03/11/2009

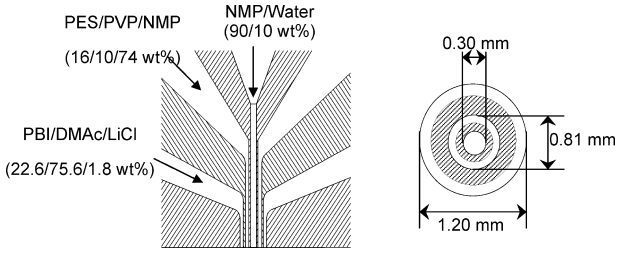

FIGURE 1. Schematic diagram of spinneret for dual-layer hollow fiber spinning.

TABLE 1. Spinning Conditions of PBI-PES/PVP Dual-Layer Hollow Fiber Membrane

external dope solution (wt%)	PBI/DMAc/LiCl (22.6/75.6/1.8)
external dope flow rate (mL/min)	0.3
inner dope solution (wt%)	PES/PVP/NMP (16/10/74)
inner dope flow rate (ml/min)	3
bore fluid composition (wt%)	NMP/water (90/10)
bore flow rate (ml/min)	1
length of air gap (cm)	10
external coagulant, temperature (°C)	tap water; 26 ± 1
dope and bore fluid temperature (°C)	26 ± 1
spinning humidity (%)	60∼70%
dimension of spinneret (mm)	$OD_1/OD_2/ID$ (1.20/0.81/0.30)
take up speed (m/min)	6

could lead to the simultaneous reconcentration of the $MgCl_2$ solution for reuse and the recovery of product water.

Materials and Methods

Fabrication and Characterizations of PBI-PES/PVP Dual-Layer Hollow Fiber Membranes. Polybenzimidazole (PBI) with a LiCl stabilizer and polyethersulfone (PES, Udel A-300) blended with polyvinylpyrrolidone (PVP of a molecular weight of 360 kDa) were used as the external and internal polymer materials, respectively for dual-layer hollow fiber membrane fabrication. N-Dimethylacetimide (DMAC) and N-methyl-2-pyrrolidone (NMP) were used as the solvents for dissolving PBI and PES materials, respectively, for the dope solutions preparation. The detailed schematic diagram of the hollow fiber spinning system has been described elsewhere (*5*) and Table 1 lists the detailed spinning conditions. The schematic of the dual-layer spinneret used in this work is shown in Figure 1. The as-spun fibers were immersed in tap water for 3 days to remove any solvent residues. To remove unblended PVP and also increase the porosity and pore size in the membrane's inner-layer, the fibers were soaked in 8000 ppm NaOCl under stirring for 24 h. After that the hollow fiber membranes were further soaked in a 50 wt% glycerol solution for 48 h under stirring. After thoroughly air drying these membranes at room temperature of 23 °C, 10 pieces of hollow fibers with a length around 20 cm each were bundled into a ϕ 3/8 in. perfluoroalkoxy (PFA) tubing and two ends were sealed with the epoxy resin to assemble a membrane module.

The morphology of the dual-layer hollow fiber membrane was observed under a field emission scanning microscopy (FESEM, JEOL JSM-6700). The detailed SEM specimen preparation was described elsewhere (*5*).

Membrane Characterization through Nanofiltration Experiments. The assembled membrane module holding 10 pieces of dual-layer hollow fibers was first subjected to the measurement of pure water permeability flux (PWP, J_o) in $L \cdot m^{-2} \cdot hr^{-1}$ (abbreviated as LMH thereafter) by an NF membrane setup described elsewhere (*8*). Subsequently, the membrane module was subjected to the 200 ppm neutral solutes (glycerol, glucose, sucrose, raffinose) and 1 mM salts (NaCl and $MgCl_2$) separation tests with different feed solutions flowing against the membrane's selective outer-layer (i.e., draw solution flows in the membrane module's shell side). The relatively low solute concentrations utilized were to avoid the occurrence of concentration polarization. Permeate was collected from the lumen side of the membrane module. All these experiments were carried out at a trans-membrane pressure of 1 bar (gauge) at room temperature. The concentrations of the neutral solute in solutions were measured with a total organic carbon analyzer (TOC ASI-5000A, Shimadzu, Japan). The single salt concentration was measured with an electric conductivity meter (Laboratory 960, Schott, Germany). The measured feed (C_f) and permeate (C_f) concentrations were used for calculating the effective solute rejection coefficient R_E (%):

$$R_E = \left(1 - \frac{C_p}{C_f}\right) \times 100\% \quad (1)$$

The relationship between Stokes radius (r_s, nm) and molecular weight (MW, g/mol) of the neutral solutes used can be expressed as (*9*)

$$\log r_s = -1.3363 + 0.395 \log MW \quad (2)$$

From eq 2, the radius (r_s) of a hypothetical solute at a given MW can be obtained. The mean effective pore size and the pore size distribution were then obtained according to the traditional solute transport approach (*2, 10*−*12*). That is by ignoring influences of the steric and hydrodynamic interaction between solute and membrane pores, the mean effective pore radius (μ_p) and the geometric standard deviation (σ_p) can be assumed to be the same as μ_s (the geometric mean radius of solute at $R_E = 50\%$) and σ_g (the geometric standard deviation defined as the ratio of the r_s at $R_E = 84.13\%$ over that at $R_E = 50\%$). Therefore, based on μ_p and σ_p, the pore size distribution of a membrane can be expressed as the following probability density function:

$$\frac{dR(r_p)}{dr_p} = \frac{1}{r_p \ln \sigma_p \sqrt{2\pi}} \exp\left[-\frac{(\ln r_p - \ln \mu_p)^2}{2(\ln \sigma_p)^2}\right] \quad (3)$$

Water Production through Forward Osmosis Tests. Forward osmosis tests on the membrane module with an effectively external membrane surface area of 60 cm^2 were conducted on a laboratory-scale setup described elsewhere (*2*). The draw solutions of $MgCl_2$ at different concentrations and feed deionized water were counter-currently pumped through the module by two peristaltic pumps with pulsation-free dampers. The draw solution was passed the membrane module once-through, whereas the feedwater circulated in the other side. The volumetric flow rates in the membrane module's lumen and shell were fixed both at 100 mL/min (corresponding to a linear velocity of 0.73 m/s in lumen and 6.73 cm/s in shell, respectively). Two different membrane orientations were tested to investigate the effect of membrane structure and concentration polarization on water permeation flux: (1) the pressure retarded osmosis (PRO) mode for when the draw solution flows directly against the PBI selective outer-layer (i.e., draw solution flows in the membrane module's shell side), and (2) the forward osmosis (FO) mode for when the draw solution flows directly against the PES/PVP supportive porous inner-layer (i.e., draw solution flows in the membrane fiber's lumen side). A digit balance recorded down the mass of water permeating from the feed into the draw solution over a selected period of time. The water permeation flux was then calculated based on the weight changes of feedwater. The product water flux (J_w) was

calculated from the slope of the feed weight change divided by the effective membrane surface area (A) as follows.

$$J_w = \frac{\Delta m}{\Delta t}\frac{1}{A} \quad (4)$$

where Δm (kg) is the permeation water weight collected over a predetermined time Δt (hr) of FO process duration.

The salt concentration in the feedwater was determined from the conductivity measurement using a calibration curve for the single salt solution. The back-flow salt flux (J_s in $g \cdot m^{-2} \cdot hr^{-1}$, abbreviated as gMH) was thereafter determined from the increase of the feed conductivity:

$$J_s = \frac{\Delta(C_t V_t)}{\Delta t}\frac{1}{A} \quad (5)$$

where C_t and V_t are the salt concentration and the volume of the feed in the end of FO tests, respectively.

Results and Discussion

Morphology Studies of the PBI-PES/PVP Dual-Layer Hollow Fiber Membrane. The newly developed dual-layer membrane has outer and inner diameters of 953 and 540 μm, respectively. Supporting Information Figure S1 shows the cross-section (CS) morphology that consists of a PBI selective outer-layer (OL) of around 10 μm, a fully porous sponge-like PES/PVP inner-layer (IL), and a delamination-free interface. Underneath the PBI selective outer-layer outer-surface (OL-OS), there are plenty of macrovoids directly and openly connected to the interface as shown in the outer-layer inner-surface (OL-IS) section as well as in the deliberately delaminated membrane structure as shown in Supporting Information Figure S1, while the outer-skin of the inner-layer (IL-OS) is fully porous. As a result, there is not much transport resistance at the interface. Since the inner-layer (IL) and the inner-layer inner-surface (IL-IS) are fully porous, the PBI outer-layer is the sole resistance and selective layer. However, as displayed in its OL photo, the average thickness of the selective layer is only about 1.5 μm if deducting the macrovoid length from the overall outer-layer thickness. As a consequence, water can rapidly diffuse across the ultrathin selective layer by the osmotic pressure gradient.

Compared to the previous single-layer PBI hollow fibers (*2*), the uniqueness of this newly developed PBI-PES/PVP dual-layer hollow fiber membranes is that not only it possesses the subnano pores and self-charged properties in the outermost PBI skin for water passage and ion rejection, but also has a sponge-like open-cell PES inner-layer with the aid of the PVP pore forming agent and the delayed demixing by the solvent-enriched bore fluid (90 wt% NMP).

Solute Rejection Characterization by Nanofiltration Tests for the PBI-PES/PVP Hollow Fiber Membrane. Figure 2 shows the solute separation, probability density, and cumulative pore size distribution curves, while Table 2 summarizes the solute rejection results on the dual-layer hollow fiber membrane under NF tests. The pure water permeability (PWP) of this membrane is only 1.74 LMH at a trans-membrane pressure of 1 bar. The pore size distribution curve as shown in Figure 2B indicates that the dual-layer hollow fiber membrane has a sharp pore size distribution. This is essential for rejecting ions and contaminants. Additional characterizations reveal that it exhibits a high rejection rate around 90% to divalent $MgCl_2$ salt and a low rejection rate of 40% to monovalent NaCl salt. Table 2 reveals the average pore radius ($\mu_p = 0.4$ nm) of the dual-layer hollow fiber membrane is just between the hydrated radius for Na^+ (0.33 nm) and Mg^{2+} (0.43 nm) (*13*). In addition to the ion size exclusion mechanism, the big difference in rejection for divalent and monovalent ions is probably also attributed to the Donnan electrostatic effect (*14*). The salts rejection data indicate the dual-layer membrane is promising for FO application on water production using $MgCl_2$ as the draw solution, but it is probably not suitable for seawater and salty water desalination since its NaCl rejection is not satisfactorily high.

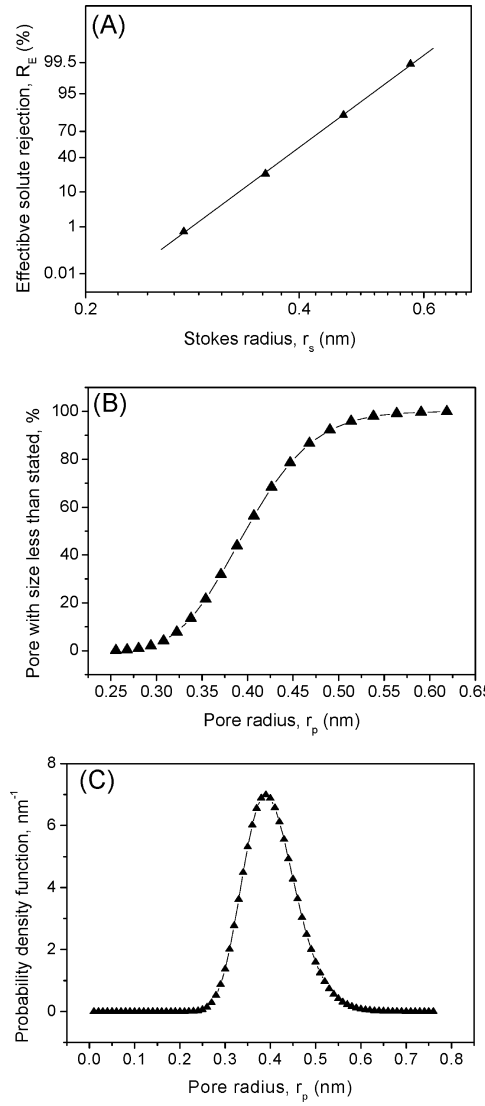

FIGURE 2. (A) Solute separation; (B) probability density; and (C) cumulative pore size distribution curves for characterizing the PBI-PES/PVP dual-layer hollow fiber FO membrane using progressively increased molecular-weight neutral sugars.

TABLE 2. Solute Rejection Results Characterized under Nanofiltration Tests on PBI-PES/PVP Dual-Layer Membrane

μ_p, nm	σ_p	MWCO, Da	PWP, LMH @ $\Delta P = 1$ bar	NaCl rejection, %	$MgCl_2$ rejection, %
0.40	1.16	338	1.74	40.02 ± 2.21	87.23 ± 0.81

Water Production via PBI-PES/PVP Dual-Layer Hollow Fiber Membrane. The dependence of water and salt fluxes on $MgCl_2$ concentration at room temperature of 23 °C at two different operation modes, namely FO and PRO, is plotted in Figure 3. It demonstrates that the water flux goes up with an increased $MgCl_2$ concentration while the salt fluxes are satisfactorily low in any circumstance. The low salt transport rate from the draw solution to the feed solution is critical for the FO process employed in any application. If draw solute is lost in water production applications, it must be replaced,

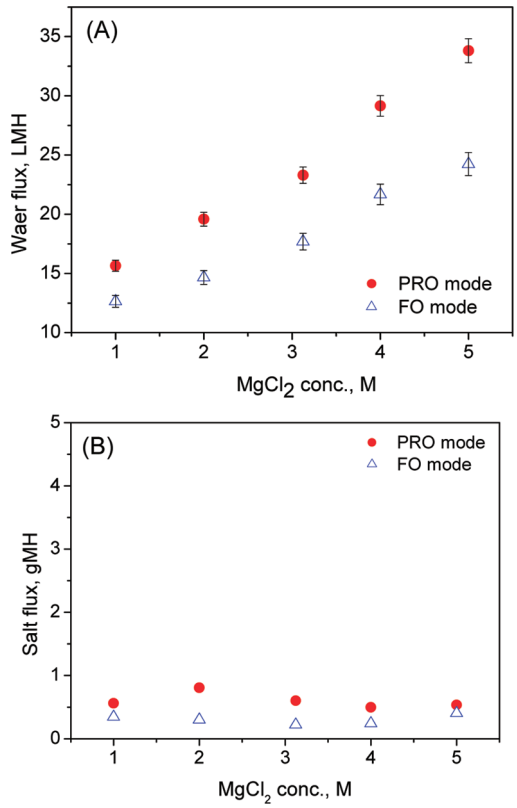

FIGURE 3. Effect of draw solution concentration on (A) water and (B) salt flux (23 ± 0.5 °C).

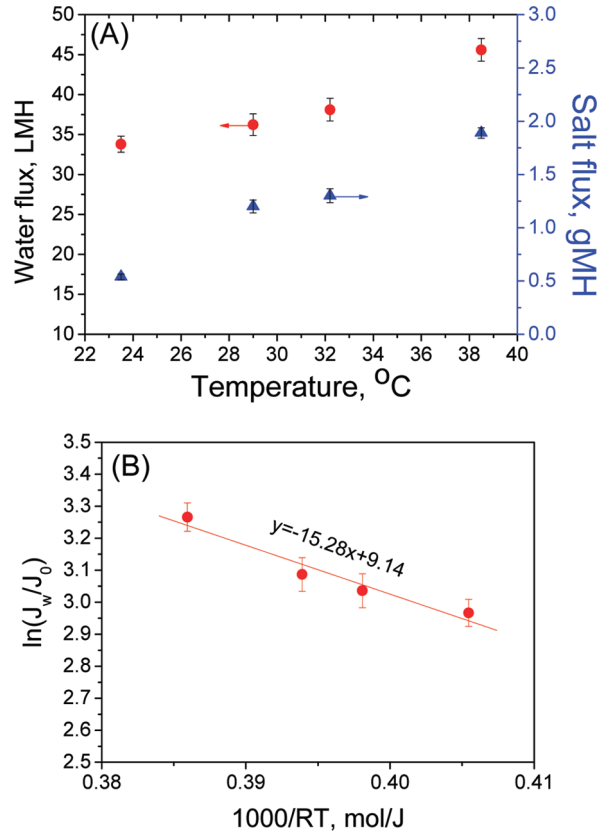

FIGURE 4. Effect of draw solution (5 M $MgCl_2$) temperature on water and salt flux operated in the PRO mode.

thereby incurring an additional cost for that water production while simultaneously contaminating the reject solution. If forward osmosis is being utilized in the concentration of fruit juice or pharmaceutical compounds, salt flux could lead to contamination of the desired product.

Generally the water flux is 4 orders of magnitude higher than the salt flux with the correspondingly same draw solution used in the FO tests. It is expected that the water flux increase with an increased draw solution concentration is mostly due to the increased effective osmotic pressure as the driving force in both operation modes. In addition, the water permeation flux in the PRO mode is much higher than that in the FO mode. This is because the net driving force reduces more significantly in the FO mode than in the PRO mode due to the severe dilutive internal concentration polarization occurred in the porous support layer (i.e., in the PES/PVP inner-layer) (*1, 2, 15–17*).

In addition, as shown in Figure 4A the water permeation flux operated in the PRO mode goes up from 33.8 LMH at 23 °C to 45.6 LMH at 38.5 °C. Meantime the salt permeation rate through the membrane is effectively low though it also increases with the operation temperature. A higher temperature can enhance the mutual diffusivities between water molecules and salt ions in the aqueous electrolyte solution. Hence, a higher operation temperature increases both water and salt fluxes across the membrane. Figure 4B shows the apparent activation energy (E_J = 15.28 kJ/mol) of the water permeation flux in the FO experiments (J_w) over the pure water permeation flux (J_o) as a function of the operation temperature (T, K) can be calculated based on the following Arrhenius equation:

$$J_w = J_0 \exp\left(\frac{-E_J}{RT}\right) \quad (6)$$

Where R is the gas constant, 8.314 J·mol^{-1}·K^{-1}.

Table 3 shows a performance comparison of the recent studies on FO processes for water production. So far, tremendous effort has been devoted by researchers in this field to identify suitable membranes and appropriate draw solutions in the FO process in order to achieve a high water flux and high salt rejection. Generally various salts or sugar solutions have been used since they are highly soluble in water and have low molecular weights, resulting in high osmotic pressures. In addition, the separation and recovery of these draw solutions can be achieved easily by precipitation, heat decomposition or RO process.

It can be seen that the most common approach to select membranes for the FO process is simply to use commercial RO membranes. Nevertheless, the main drawback of this practice is the limited flux achieved. It is less than 10 LMH in most FO processes for seawater desalination since the RO membranes are relatively thick by necessity to withstand the hydraulic pressure. It was reported recently by peeling off the support fabric from RO membrane for FO tests, the flux of this RO membrane without fabric could increase dramatically from several LMH to 36 LMH (*18*). Although the strategy is promising for flux enhancement, the practice is not feasible in large scale membrane preparations for the FO process.

Hydration Technologies Inc. (HTI, previously Osmotek Inc.) is the market leader in membrane fabrications for the FO process. It has substituted the fabric support in the traditional RO membrane by an embedded polyester mesh and developed a specific FO membrane with a maximized water flux while maintaining the desired salt rejection. The membrane thickness is less than 50 μm and this membrane has been widely tested in water reclamation in space (*19, 20*), osmotic membrane bioreactor for water recovery (*21*), power generation (*22*), and seawater desalination (*23*). Recent work conducted in Elimelech's research group demonstrates when water was used as the feed and 1.5 M NaCl as the draw solution, the flux can reach above 40 LMH (*16, 18*). Nevertheless, it was reported that the cellulose triacetate,

TABLE 3. Overview of Recent Research on FO Process with Different Membranes

operation temp (°C)	feed	draw	draw flow rate	operation mode	membrane	flux (LMH)	ref
23	DI water	5 M MgCl2	0.73 m/s	FO	dual-layer (PBI-PES/PVP) NF membrane	24.2	this work
23	DI water	5 M MgCl2	6.73 cm/s	PRO	dual-layer (PBI-PES/PVP) NF membrane	33.8	this work
38.5	DI water	5 M MgCl2	0.73 cm/s	PRO	dual-layer (PBI-PES/PVP) NF membrane	45.6	this work
22.5	DI water	5 M $MgCl_2$	0.56 cm/s	PRO	PBI hollow fiber membrane	11.0	*2*
67.0	3.5% NaCl	45% Na_2HPO_4			RO membrane (AG), GE Osmonics	2.5	*24*
67.0	3.5% NaCl	45% Na_2HPO_4			RO membrane (AD), GE Osmonics	1.1	*24*
69.0	3.5% NaCl	45% Na_2HPO_4			Gore-Tex PTFE membrane, Gore	4.1	*24*
69.0	3.5% NaCl	45% Na_2HPO_4	36 L/hr	PRO	cellulose triacetate RO membrane, Osmotek	14.5 (degraded at pH 9)	*24*
ambient temperature	water	98 g/L anonymous osmotic agent			FO membrane, Hydration Technologies	24.0	*19*
50.0	0.5 M NaCl	4 M NH_4HCO_3	4.17 cm/s	PRO	FO membrane, Hydration Technologies	11.0	*15*
22.5	DI water	0.5 M NaCl	30 cm/s	PRO	FO membrane, Hydration Technologies	18.6	*17*
50.0	0.05 M NaCl	6 M NH_4HCO_3	30 cm/s	PRO	FO membrane, Hydration Technologies	36.0	*25*
25.0	digester centrate	70 g/L NaCl	1.5 L/min	FO	FO membrane, Hydration Technologies	16.4	*26*
50.0	0.5 M NaCl	5 M fructose	8.34 cm/s	PRO	FO membrane, Hydration Technologies	19.5	*27*
20.0	DI water	0.5 M NaCl	5.5 L/min	FO	FO membrane, Hydration Technologies	8.50	*21*
20.0	activated sludge	4.5 M NaCl	5.5 L/min	FO	FO membrane, Hydration Technologies	12.9	*21*
20.0	DI	1.5 M NaCl	21.3 cm/s	PRO	polyamide RO membrane with the fabric removed, Dow Filmtec	8.1	*18*
20.0	DI water	1.5 M NaCl	21.3 cm/s	PRO	cellulosic RO membrane with the fabric removed, GE Osmonics	36.0	*18*
20.0	DI water	1.5 M NaCl	21.3 cm/s	PRO	FO membrane, Hydration technologies	43.2	*16, 18*

the membrane material of HTI FO membrane was not stable in alkaline solutions and would degrade at pH 9 (*24*).

In contrast, the dual-layer hollow fiber membrane developed in this work could be operated as a forward osmosis membrane under harsh environment since both PBI and PES materials have superior chemical resistance. Figure 3 shows that the membrane can reach almost 34 LMH water flux and 10^4 times less of salt flux when it is operated in the PRO mode. It should be mentioned that the relatively high flux was achieved with a very low draw solution crossflow rate which the peristaltic pumps could sustain and at a nonelevated operation temperature. Table 3 reveals the water flux can easily enhance to more than 45 LMH if the operation temperature slightly increases to 38.5 °C. The water fluxes of this dual-layer FO membrane achieved by using $MgCl_2$ as the draw solution are better than most commercial RO membranes and comparable to those achieved by commercial HTI FO membrane using other sugar or salts as draw solutes. It is expected that by tailoring dual-layer membrane structures, especially by further reducing its selective skin thickness, minimizing the porosity and also the thickness of the support layer and optimizing hydrodynamic flow conditions in the FO process, the water flux can be further enhanced.

Acknowledgments

We thank the National University of Singapore and the National Research Foundation, Singapore for funding this project with the grants of R-279-000-249-646 and R-279-000-271-272. Special thanks are due to PBI Performance Products Inc., USA for providing polybenzimidazole (PBI) materials. We are also very grateful to the reviewers' enlightening

suggestions to help improve the scientific quality of this work significantly.

Appendix A

NOMENCLATURE

A	the effective membrane surface area, cm^2
C_f	solute concentration in the feed solution, mol/L
C_p	solute concentration in the permeate, mol/L
C_t	salt concentration, mol/L
E_j	the apparent activation energy, kJ/mol
J_o	the pure water permeation flux, $L \cdot m^{-2} \cdot hr^{-1}$
J_w	the product water flux, $L \cdot m^{-2} \cdot hr^{-1}$
J_s	the back flow salt flux, $g \cdot m^{-2} \cdot hr^{-1}$
Δm	the permeation water weight gain, kg
MW	molecular weight, g/mol
r_p	the membrane pore size, nm
r_s	solute Stokes radius, nm
R_E	effective solute rejection rate, %
R	gas constant, 8.314 $J \cdot mol^{-1} \cdot K^{-1}$
Δt	the operation time interval, hr
T	operation temperature, K
V_t	the volume of the feed at a time interval of Δt

Greek

μ_p	the mean effective pore radius, nm
μ_s	the geometric mean radius of solute at $R_E = 50\%$).
σ_p	the geometric standard deviation
σ_g	the geometric standard deviation defined as the ratio of the r_s at $R_E = 84.13\%$ over that at $R_E = 50\%$

Supporting Information Available

SEM images of PBI-PES/PVP dual layer FO membrane. This material is available free of charge via the Internet at http://pubs.acs.org.

Literature Cited

(1) Cath, T. Y.; Childress, A. E.; Elimelech, M. Forward osmosis: Principles, applications, and recent developments. *J. Membr. Sci.* **2006**, *281*, 70–87.

(2) Wang, K. Y.; Chung, T. S.; Qin, J. J. Polybenzimidazole (PBI) nanofiltration hollow fiber membranes applied in forward osmosis process. *J. Membr. Sci.* **2007**, *300*, 6–12.

(3) Jiang, L. Y.; Chung, T. S.; Cao, C.; Huang, Z.; Kulprathipanja, S. Fundamental understanding of nano-sized zeolite distribution in the formation of the mixed matrix single- and dual-layer asymmetric hollow fiber membranes. *J. Membr. Sci.* **2005**, *252*, 89–100.

(4) Li, Y.; Chung, T. S.; Huang, Z.; Kulprathipanja, S. Dual-layer polyethersulfone (PES)/BTDA-TDI/MDI co-polyimide (P84) hollow fiber membranes with a submicron PES-zeolite beta mixed matrix dense-selective layer for gas separation. *J. Membr. Sci.* **2006**, *277*, 28–37.

(5) Li, D. F.; Chung, T. S.; Wang, R. Morphological aspects and structure control of dual-layer asymmetric hollow fiber membranes formed by a simultaneous co-extrusion approach. *J. Membr. Sci.* **2004**, *243*, 155–175.

(6) Widjojo, N.; Chung, T. S.; Krantz, W. B. A morphological and structural study of Ultem/P84 copolyimide dual-layer hollow fiber membranes with delamination-free morphology. *J. Membr. Sci.* **2007**, *294*, 132–146.

(7) Lafreniere, L.; Talbot, F. D. F.; Matsuura, T.; Sourirajan, S. Effect of PVP additive on the performance of PES ultrafiltration membrane. *Ind. Eng. Chem. Res.* **1987**, *26*, 2385–2389.

(8) Wang, K. Y.; Matsuura, T.; Chung, T. S.; Guo, W. F. The effects of flow angle and shear rate within the spinneret on the separation performance of poly(ethersulfone) (PES) ultrafiltration hollow fiber membranes. *J. Membr. Sci.* **2004**, *240*, 67–79.

(9) Bowen, W. R.; Mohammad, A. W. Characterization and prediction of nanofiltration membrane performance-A general assessment. *Trans I Chem E. Part A*, **1998**, *76*, 885–893.

(10) Michaels, A. S. Analysis and prediction of sieving curves for ultrafiltration membranes - a universal correlation. *Sep. Sci. Technol.* **1980**, *15*, 1305–1322.

(11) Youm, K. H.; Kim, W. S. Prediction of intrinsic pore properties of ultrafiltration membrane by solute rejection curves - Effects of operating-conditions on pore properties. *J. Chem. Eng. Jpn.* **1991**, *24*, 1–7.

(12) Singh, S.; Khulbe, K. C.; Matsuura, T.; Ramamurthy, P. Membrane characterization by solute transport and atomic force microscopy. *J. Membr. Sci.* **1998**, *142*, 111–127.

(13) Nightingale, E. R. Phenomenological theory of ion salvation-Effective radii of hydrated ions. *J. Phys. Chem.* **1959**, *63*, 1381–1387.

(14) Donnan, F. G. Theory of membrane equilibria and membrane-potentials in the presence of non-dialyzing electrolytes - a contribution to physical-chemical physiology. *J. Membr. Sci.* **1995**, *100*, 45–55.

(15) Ng, H. Y.; Tang, W. L.; Wong, W. S. Performance of forward (direct) osmosis process: Membrane structure and transport phenomenon. *Environ. Sci. Technol.* **2006**, *40*, 2408–2413.

(16) McCutcheon, J. R.; Elimelech, M. Influence of concentrative and dilutive internal concentration polarization on flux behavior in forward osmosis. *J. Membr. Sci.* **2006**, *284*, 237–247.

(17) Gray, G. T.; McCutcheon, J. R. M. Elimelech. Internal concentration polarization in forward osmosis: role of membrane orientation. *Desalination* **2006**, *197*, 1–8.

(18) McCutcheon, J. R.; Elimelech, M. Influence of membrane support layer hydrophobicity on water flux in osmotically driven membrane processes. *J. Membr. Sci.* **2008**, *318*, 458–466.

(19) Cath, T. Y.; Gormly, S.; Beaudry, E. G.; Flynn, M. T.; Adams, V. D.; Childress, A. E. Membrane contactor processes for wastewater reclamation in space Part I. Direct osmotic concentration as pretreatment for reverse osmosis. *J. Membr. Sci.* **2005**, *257*, 85–98.

(20) Cath, T. Y.; Adams, D.; Childress, A. E. Membrane contactor processes for wastewater reclamation in space II. Combined direct osmosis, osmotic distillation, and membrane distillation for treatment of metabolic wastewater. *J. Membr. Sci.* **2005**, *257*, 111–119.

(21) Cornelissen, E. R.; Harmsen, D.; Korte, K. F. D.; Ruiken, C. J.; Qin, J. J.; Oo, H.; Wessels, L. P. Membrane fouling and process performance of forward osmosis membranes on activated sludge. *J. Membr. Sci.* **2008**, *319*, 158–168.

(22) McGinnis, R. L.; McCutcheon, J. R.; Elimelech, M. A novel ammonia-carbon dioxide osmotic heat engine for power generation. *J. Membr. Sci.* **2007**, *305*, 13–19.

(23) McCutcheon, J. R.; McGinnis, R. L.; Elimelech, M. A novel ammonia-carbon dioxide forward (direct) osmosis desalination process. *Desalination.* **2005**, *174*, 1–11.

(24) Miller J. E.; Evans L. R. *Forward Osmosis: A New Approach to Water Purification and Desalination*; Sandia National Laboratories Report: Albuquerque, NM, 2006.

(25) McCutcheon, J. R.; McGinnis, R. L.; Elimelech, M. Desalination by ammonia-carbon dioxide forward osmosis: Influence of draw and feed solution concentrations on process performance. *J. Membr. Sci.* **2006**, *278*, 114–123.

(26) Holloway, R. W.; Childress, A. E.; Dennett, K. E.; Cath, T. Y. Forward osmosis for concentration of anaerobic digester centrate. *Water Res.* **2007**, *41*, 4005–4014.

(27) Tang, W. L.; Ng, H. Y. Concentration of brine by forward osmosis: Performance and influence of membrane structure. *Desalination.* **2008**, *224*, 143–153.

ES803360T